Received: May 10, 2023. Revised: June 11, 2023.

International Journal of
Intelligent Engineering & Systems

http://www.inass.org/

Multi-Scale Learning with Attention-based UNet and Marginal Space Deep Ambiguity Transfer Learning for Lung Disease Prediction

Jinu Paulson Siluvai Rathinam[1]* **Angeline Prasanna Gopalan[1]**

[1]*Department of Computer Science, AJK College of Arts and Science, Coimbatore - 641105, TamilNadu, India*
*Corresponding author's Email: jinuplsn7phd@gmail.com

Abstract: Early identification of lung-infected persons is crucial. To achieve this, lung computed tomography (CT) scan segmentation and categorization models have been broadly developed for COVID-19 diagnosis. However, these models are not always able to classify appropriate risk levels when quantifying tissues from diseased regions, they need more relevant and discriminative features to classify disease risk levels. Therefore, this paper designs a new transfer learning (TL) based deep model named multi-scale function learning with an attention-based UNet and marginal space deep ambiguity attentive transfer learning (MS-AUNet-MSDATL). In the first step, lung CT and X-ray images from the dataset are collected. The MS-AUNet-MSDL system takes such images, enriches them with the multi-structure response filter (MSRF), and then divides them into ROIs for diseased and healthy tissue at different scales. After that, the regions of interest (ROIs) for the afflicted tissue are input into the trained CNN structures to extract features. In addition, the CNN-LSTM classifier is used to train the extracted features and obtain the learned classification models. Test scans are classified as low, medium, or high-risk using the learned classifiers to ensure an accurate COVID-19 diagnosis. The epistemic ambiguity is calculated using the classification error. Then, the ambiguity is given as feedback to the classifier to improve the accuracy. Finally, the experimental outcomes revealed that the MS-AUNet-MSDATL on the chest CT image dataset achieves 97.34% accuracy, which is 14% higher than Distant Domain TL (DDTL), 12.4% higher than self-supervised super sample decomposition TL (4SD-TL), and 10.4% higher than the two-stage TL method (TL-Med). Also, the MS-AUNet-MSDATL on the chest X-ray image dataset achieves 97.18% accuracy, which is 16.8% higher than DDTL, 14.3% higher than 4SD-TL, and 10.5% higher than the TL-Med.

Keywords: COVID-19 diagnosis, CT imagery, X-ray imagery, MS-AUNet-MSDL, Transfer learning, Pre-learned CNN, Ambiguity estimation, Disease risk level, LSTM.

1. Introduction

The novel coronavirus disease (COVID-19) that was responsible for the lung infection pandemic that began in 2020 first manifested itself and spread quickly over the planet [1]. Respiratory infections are the main cause of COVID-19-related rheumatic fever. Additionally, it might result in intestinal infections, which can produce digestive symptoms like nausea, vomiting, and diarrhea [2, 3]. The world health organization (WHO) [4] estimates that as of September 26, 2022, there were 612,236,677 recorded incidents of new coronary pneumonia globally, with 6.51 million deaths. Timely identification of COVID-19 victims may help in restricting the virus's evolution because COVID-19 is highly infectious [5].

So, a prompt and correct diagnosis of COVID-19 is essential for the earlier diagnosis of the infection [6-8]. A statistical analysis of COVID-19 evolution by CT scans is possible since they reveal COVID-19's key morphological features [9]. The advantage of chest CT scans over X-rays is that they are more effective at identifying respiratory problems [10, 11]. Pulmonary CT scans are suggested by clinicians as the main pulmonary therapeutic screening tool. The traditional diagnosis of irregularities by doctors necessitates a significant amount of time and is greatly impacted by their judgment, hence it is crucial to research and develop

an effective automated system for clinical visual classification. It can support medical professionals in making accurate real-time diagnoses and treatment choices.

Deep learning approaches were incredibly successful at separating the required region-of-interest (ROI), like healthy and unhealthy pulmonary areas, from CT scans [12, 13]. The correct delineation of the COVID-19 disease patch using deep learning approaches is vitally pertinent for quick detection and estimation by physicians. To segment the COVID-19 CT images, an Attention-based U-Net (AUNet) model [14] was created to reweight the characteristic representation and capture the rich contextual characteristics, the spatial and channel attention units in U-Net employ an attention technique. To capture properties at different dimensions, a residual unit with dilated convolutions was also used. Additionally, the tiny irregular patches in the CT scans were segmented using the focal Tversky error. In contrast, the lung CT images' segregation of unclear edges was unsatisfactory.

Hence in this article, an MS-AUNet-MSDATL framework is proposed to simultaneously segregate the COVID-19 infected ROIs and classify the disease risk levels from the CT and X-ray scans. In this framework, initially, multi-scale function learning with AUNet is created to extract features at various locations. Then, an improved filter MSRF is added to the attention-based U-Net to improve segmentation effectiveness and acquire structural information from the CT and X-ray images. Next, marginal learning of the bounding box variables is minimized into sub-spaces to detect the target tissues. Finally, the segmented ROIs from the MS-AUNet structure are given to the different pre-learned CNN models like VGG16, ResNet50, InceptionResNetV2, and DenseNet121 structures. These pre-learned models can hierarchically capture more informative and discriminative characteristics from the lung CT and X-ray scans. Those characteristics are provided to the CNN-LSTM classifier to classify the disease risk levels for proper diagnosis. Moreover, the epistemic ambiguity of categorization outcomes is measured to determine areas where the learning frameworks are not optimistic regarding their decisions. Thus, the measured ambiguities deliver useful data regarding where and how much the physician could believe the classifier forecasts for COVID-19 recognition and diagnosis.

The remaining portions of this paper are outlined: Section 2 reviews earlier research on the categorization approaches for COVID-19 CT and X-ray scans. The operation of the MS-AUNet-MSDATL framework is described in section 3, and its effectiveness is demonstrated in section 4. Section 5 outlines the research's general findings and suggests innovative solutions.

2. Literature survey

An automated deep TL-based scheme was developed [15] to identify COVID-19 disease in chest X-rays by utilizing the Xception structure. But its accuracy was not efficient due to the poor quality of chest X-ray scans, resulting in misclassification. DDTL was developed [16] for COVID-19 diagnosis by considering unannotated chest X-ray image databases as the source data and a limited collection of COVID-19 lung CT as the target data. Conversely, the limitations of this model were (i) it tends to be case-specific, (ii) the choice of source data was very difficult in a few scenarios and (iii) distant attribute mining obtain low precision.

A dense CNN-based TL [17] was designed to monitor COVID-19-suspected patients using chest X-ray scans. A modified multi-crossover genetic algorithm (MMCGA) was applied to optimize the hyperparameters. But, its accuracy was degraded due to the noisy and poor visibility scans. A method called 4SD-TL [18] was presented to annotate unannotated chest X-ray scans and enhance the robustness of domain adaptation using a downstream training with a class-decomposition layer. But the accuracy was not efficient if the parameters were not selected properly.

The TL-based COVID-19 monitoring scheme [19] was presented which executes truncated VGG16 to forecast COVID-19 CT images. The VGG16 structure was modified to capture features from CT scans. Then, a principal component analysis (PCA) was applied to choose the most relevant characteristics, which were classified by the bagging ensemble with the SVM to identify COVID-19 patients. But the accuracy was less due to ineffective segmentation of diseased lung ROIs.

A 3-stage identification system [20] was designed to enhance the accuracy of detecting COVID-19 from lung CT images. In the initial stage, data augmentation was performed by the stationary wavelets. In the second stage, a pre-learned CNN was applied to detect COVID-19 cases. In the third stage, irregularities in the CT images were localized by the feature map and activation layers of the pre-learned CNN model. But it has a less precision while increasing the number of COVID-19 images.

TL with fine-tuning on a deep CNN-based ResNet50 framework [21] was developed to

categorize COVID-19 patients from chest X-ray scans. To do this, the ResNet50 structure was altered by including additional 2 fully connected layers and utilizing various pre-learned weights. But, it needs to identify the ROI of COVID-19 in X-ray scans for enhancing accuracy.

A method to automatically categorize COVID-19 by various pre-learned CNN and sparrow search algorithms (SSA) [22] was designed using CT lung scans. The SSA was applied to fine-tune various CNN and TL hyperparameters to obtain the optimal configuration for the pre-learned framework. However, an ensemble classifier was needed to increase the classification accuracy.

A TL-Med method [23] was designed for detecting COVID-19. Initially, the vision transformer (ViT) pre-learning system was utilized to get generic characteristics from huge heterogeneous data and the medical characteristics were learned from large-scale homogeneous data. Moreover, two-phase TL was applied to use the trained key characteristics and the actual data for COVID-19 identification. But, the accuracy was reduced because the augmented annotated samples have negative effects on pre-learning.

A novel stacked CNN framework [24] was developed for automatically recognizing COVID-19 illness from chest CT and X-ray scans. Various sub-models were acquired from the VGG19 and the Xception frameworks during learning. After that, those frameworks were combined by the softmax categorizer, which fuses the discriminating power of various CNN sub-models and identifies COVID-19 illness. But, it needs to categorize X-ray scans into the different classes of pneumonia.

MSDTL [25] was developed to effectively monitor the prospective COVID-19 diseases. In this method, every province-related database was trained on a basic long short-term memory (LSTM) framework for forthcoming disease prediction in that domain. Also, the learned framework was fine-tuned by the MSDTL to achieve precise prediction. But, the accuracy was degraded while the disease risk level was extremely low.

A new ensemble model [26] was developed which combines the power of various CNN structures before arriving at the final decision. Different pre-learned frameworks were applied and fine-tuned by the lung CT images. Then, those frameworks were utilized to build a robust ensemble categorizer, which provides the final forecasting outcome. However, the recognition of various lung diseases from CT images was required to increase the accuracy.

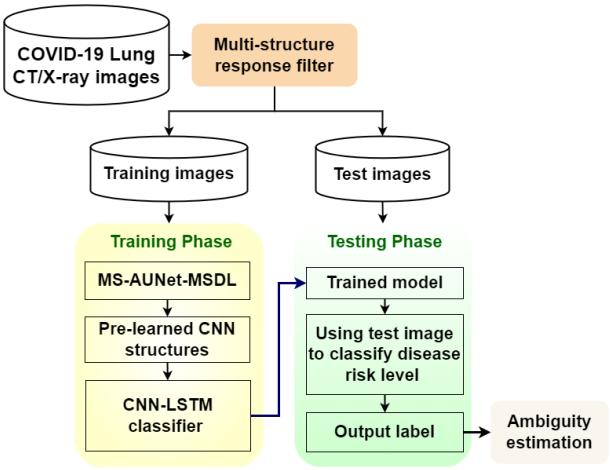

Figure. 1 Overall pipeline of the presented study

2.1 Research contribution

This research focuses on segmenting COVID-19-infected ROIs from the lung CT and X-ray images and classifying the infection risk levels simultaneously by learning disease features using an ensemble classifier for achieving an effective diagnosis.

In contrast with the literature frameworks, the proposed work can be useful for physicians to accurately identify disease risk levels and provide appropriate diagnosis strategies timely.

3. Proposed methodology

In this section, the presented MS-AUNet-MSDATL to categorize the risk levels of COVID-19 is explained briefly. An overall pipeline of the presented study is portrayed in Fig. 1.

The key tasks in this framework include:

1. First, COVID-19 lung CT and X-ray scans are collected from different open sources. Such scans are enriched by the MSRF and segregated into the COVID-19-infected tissue ROIs and healthy ROIs at multiple scales by the MS-AUNet-MSDL.
2. Then, those infected tissue ROIs are fed to the pre-learned CNN structures for extracting more relevant and discriminative features.
3. Moreover, the extracted features are passed to the CNN-LSTM classifier to train those features and get the trained classification models.
4. The trained classifiers are used to classify the test scans into low, medium, and high-risk levels for proper COVID-19 diagnosis.

The below sections describe the TL-based COVID-19 disease risk level categorization.

3.1 Transfer learning-based disease risk level categorization

In this study, the TL method is employed to learn the CNN-LSTM classifier for categorizing lung disease (COVID-19) risk levels. The main ideas of the TL are domains (different datasets) and tasks (classification). A specific domain (dataset) D in TL has a feature space X and a marginal probability distribution $P(X)$. So, this domain is defined by Eq. (1).

$$D = \{X, P(X)\} \tag{1}$$

A task T (classification) in TL has a label space Y and a target classification function $f(X)$, which is represented by conditional probability $P(Y|X)$. This is provided by Eq. (2).

$$T = \{Y, P(Y|X)\} \tag{2}$$

The source domain is considered to train the classification model and the target domain is applied to categorize the images using the source domain model.

- Condition: For a source domain (D_s) and a learning task on D_s (T_s), a target domain (D_t) and a learning task (T_t) on D_t.
- Aim: Utilize the knowledge of D_s and T_s to enhance the learning of the classification function $f(\cdot)$ on D_t.
- Constraints: $D_s \neq D_t$, $T_s \neq T_t$

This presented system entirely relies on the relevant and discriminative features of CT and X-rays scans to classify the risk levels of COVID-19 disease. Various CNN structures pre-learned on the ImageNet database are considered and adapted for COVID-19 disease risk level categorization. Such networks are VGG16, ResNet50, InceptionResNetV2 and DenseNet121 structures.

Learning such CNN structures is computationally complex since they contain several layers and learnable variables. The major assumption in this system is that there are key similarities between image recognition processes and the risk level categorization of COVID-19 from CT and X-ray scans. As a result, the learning task may be quickened by properly applying the knowledge from the first one to the second. Although each pre-learned structure is formed by non-medical pictures, it is plausible that the manipulation of the CT and X-ray scan pixels by these networks might allow the categorization task.

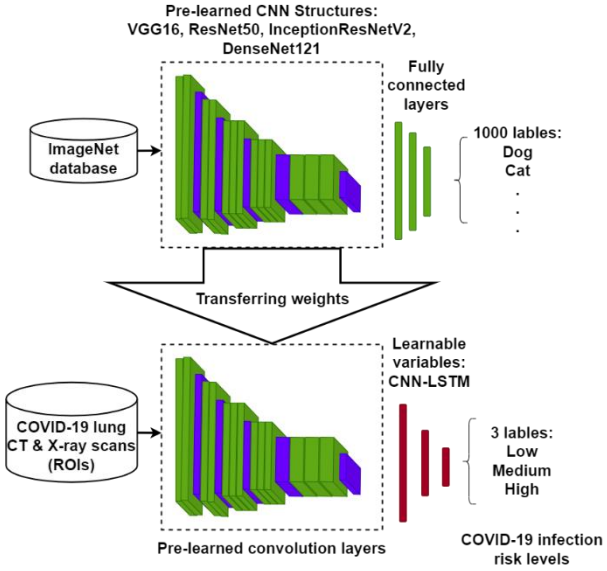

Figure. 2 Block diagram of TL-based COVID-19 infection risk level classification

As portrayed in Fig. 2, the variables of the convolutional layers are maintained constant in the learning task. Every COVID-19-infected ROI of the CT and X-ray scans from the MS-AUNet-MSDL is provided to the convolutional layers of such 4 pre-learned networks for hierarchically extracting various features. After that, the back end of those structures is substituted by the CNN-LSTM classifier to classify the risk levels of COVID-19 illness. The pooling function in the final convolutional layer of such pre-learned structures is neglected to prevent discarding relevant characteristics before providing them to the categorization frameworks.

3.1.1. Pre-learned CNN structures

This section describes the considered pre-learned CNN structures to obtain characteristics.

- VGG16 structure: This structure, which resembles AlexNet, is made up of 13 convolutional, nonlinear filtering, pooling, nonlinear filtering, pooling, and 3 fully connected layers. The convolution channel's filter dimension is 3×3 and the pooling dimension is 2×2. This model outperforms AlexNet because of its basic design [27].
- ResNet50 structure: The most often employed deep structure for multiclass categorization is the residual convolutional network (ResNet) [28]. It can provide an immediate connection to its previous layers by residual blocks. This enables the gradient

Table 1. Summary of pre-learned structures utilizing for transfer learning

Structure	Input dimension	No. of features	No. of variables
VGG16	224 × 224	25088	14714688
ResNet50		100352	23587712
DenseNet121		50176	7037504
InceptionResNetV2	299 × 299	98304	54336736

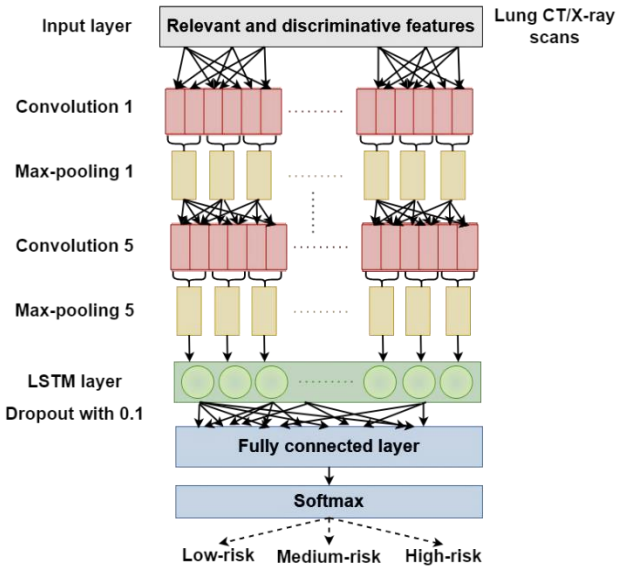

Figure. 3 Structure of CNN-LSTM

flow in the backpropagation method.

- InceptionResNetV2 structure: It prevents overfitting issues by utilizing inception blocks. Also, it utilizes residual blocks and constructs InceptionResNetV2 [29], which combines both residual and inception blocks.
- DenseNet121 structure: In DenseNet, each layer obtains every feature map from preceding layers as input, which enables the network to reduce the number of variables and avoid gradient vanishing [30].

Table 1 provides a summary of such pre-learned structures. As portrayed in Fig. 2, model weights are maintained constant in the TL process. The dimension of the given input scans is 224×224 for VGG16, ResNet50, and DenseNet121, whereas the input dimension of the InceptionResNetV2 structure is 299×299.

3.2 CNN-LSTM classifier

The COVID-19 infection risk level classification is a 3-class categorization problem, where the input is the lung CT or X-ray scan ROIs and the result is the label defining the risk levels of COVID-19 infection. Initially, the scans are processed by the convolutional layers of 4 pre-learned CNN models. After that, hierarchically obtained characteristics are processed by the CNN-LST classifier (as depicted in Fig. 3, which comprises CNN and LSTM layers for the categorization task.

The input layer consists of 5 CNN layers, each layer followed by the max-pooling to process the given characteristics. The first two CNN layers are made up of 64 and 128 kernels, each having a kernel size of three, and a maximum pooling size of two.

The following two CNN layers use max-pooling with a pool size of four and 256 and 512 kernels with a kernel size of three. The final CNN layer is made up of 1024 kernels with a kernel size of three and a maximum pooling size of six. The output of the final CNN layer is passed to the LSTM layer, which has 60 memory units. Also, a dropout is used to regularize LSTMs and avoid overfitting issues.

The LSTM network layer comprises the input gate, forget gate and output gate. The forget gate is used to calculate a degree of forgetting a feature preceded by the current LSTM unit as Eq. (3):

$$f_t = \sigma\left(W_f \cdot [h_{t-1}, x_t] + b_f\right) \tag{3}$$

In Eq. (3), W_f, b_f are the weight vector and bias value of the forget layer, respectively. σ is the sigmoid activation function, x_t is the input feature in the input gate, f_t is the forget gate, and h_{t-1} is the result of a previous hidden state.

The input gate is used to determine how much present feature is contained in the image as Eqs. (4), and (5):

$$i_t = \sigma(W_i \cdot [h_{t-1}, x_t] + b_i) \tag{4}$$

$$\tilde{C}_t = tanh(W_C \cdot [h_{t-1}, x_t] + b_C) \tag{5}$$

Here, W_i, W_C are the weight vector of the input gate and neuron condition vector, respectively. b_i, b_C are the bias values of the input gate and neuron condition vector, respectively. $tanh$ is the hyperbolic tangent activation function, $i_t, \tilde{C}_t$ are the input gate, and the updated new cell state, respectively.

Once the features traverse via the input and forget gates, the LSTM fine-tunes their units to determine the outcome of the current LSTM unit and pass it to the consecutive LSTM unit as Eq. (6):

$$C_t = f_t * C_{t-1} + i_t * \tilde{C}_t \tag{6}$$

In Eq. (6), C_t is the current cell state, and C_{t-1} is

the old cell state. The output gate merges the present input and LSTM unit to compute the result of the present LSTM unit as Eqns. (7) and (8):

$$o_t = \sigma(W_o \cdot [h_{t-1}, x_t] + b_o) \quad (7)$$

$$h_t = o_t * tanh(C_t) \quad (8)$$

In Eqs. (7) and (8), h_t represent the hidden state that serves as the solution of the block over t, o_t is the output gate, W_o and b_o are the weight vector and bias value of the output gate, respectively.

The resultant feature maps from the LSTM layer are passed to the fully connected layer followed by the softmax activation function for the classification of COVID-19 infection risk levels. A fully connected layer uses conditional probability to get an absolute feature map. Softmax $\big(P(C,b)\big)$ is a probability of features of a certain image belong to a given class C. It is determined by Eq. (9).

$$P(C,b) = \frac{P(b,C)\times P(C)}{\sum_{N=1}^{C}(N)\times P(b,N)} \quad (9)$$

In Eq. (9), $P(C)$ is class probability, C is the total number of classes (i.e., low-risk, medium-risk, and high-risk). Eq. (9) is rewritten as Eq. (10):

$$softmax = P(C,b) = \frac{e^{\beta^C[b]}}{\sum_{N=1}^{C} e^{\beta^N[b]}} \quad (10)$$

$$\text{Where } \beta^C[b] = \ln[P(b,C)\times P(C)] \quad (11)$$

3.3 Ambiguity estimation

In this study, epistemic ambiguity is considered since it nearly associates with the generalization power of networks for novel scans. An ensemble of various networks is used to get ambiguities related to the qualitative findings. An ensemble has many networks established by various structures, categories, and sampled subgroups.

The generalization capability of networks varies depending on how each network is developed. The absolute outcome is derived by combining the results of each network. The epistemic ambiguity might be calculated using the classification error. The classification entropy is computed as a metric of the epistemic ambiguity, which estimates the ambiguity in results made by each network. The ensemble epistemic ambiguity is computed as the entropy of the average posterior probability:

$$\hat{p}(y|x) = \frac{1}{N}\sum_{i=1}^{N} p_{\theta_i}(y|x) \quad (12)$$

$$H\big(\hat{p}(y|x)\big) = \sum_{i=0}^{C} \hat{p}(y_i|x)\log\hat{p}(y_i|x) \quad (13)$$

In Eq. (13), θ_i denotes the group of variables for i^{th} network part and C varies over each label. Consider a scenario when each CNN-LSTM classifies that an input corresponds to label 2 (high risk) with α% chance, label 1 (medium risk) with β%, and label 0 (low risk) with γ% chance for specific input.

When this process is continued multiple times for the given input, it is comparable to ensembling many frameworks to predict the final probability, which is determined by Eq. (12). Suppose the mean probability classifies that an input corresponds to labels 2, 1, and 0 with 0.5, 0.2 and 0.3, correspondingly. According to Eq. (13), the classification entropy is computed by $0.5\log(0.5) + 0.2\log(0.2) + 0.3\log(0.3)$. It is observed that the classification entropy equals 0 if the result is allocated to a label with a greater chance and equals high if the network structure is unaware of its result.

4. Experimental results

In this section, the performance of the MS-AUNet-MSDATL is measured and evaluated with existing methods from referred papers such as DDTL [16], 4SD-TL [18] and TL-Med [23] and the proposed concepts both are implemented in MATLAB 2017b for conducting a comparative analysis in terms of precision, recall, f-measure, and accuracy. Two datasets Dara1400 Covid19 Xray dataset and radiopaedia-COVID-19 CT dataset are used in this paper for experimental purpose.

4.1 Dataset

In this experiment, the Dara1400Chest X-ray image dataset [31] is used. From this dataset, a total of 1200 chest X-ray images belonging to healthy and COVID-19. For training 300 healthy and 300 COVID-19 are used and 300 images from each class is used for testing.

Also, the Radiopaedia-COVID-19 CT Cases-2020 dataset [32] is considered. From this dataset, a total of 760 COVID-19 chest CT images and 760 normal chest CT images. For training, 380 images from each class are considered and 380 images from each class are considered for testing.

4.2 Accuracy

It is the proportion of COVID-19 examples properly categorized over the total number of examples tested. It is calculated by Eq. (14).

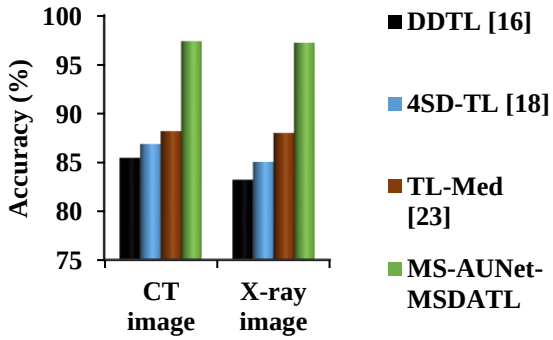

Figure. 4 Comparison of accuracy

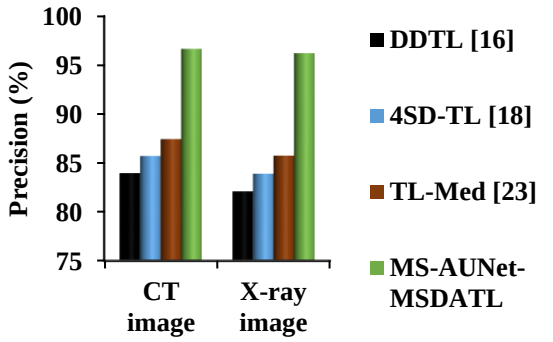

Figure. 5 Comparison of precision

$$Accuracy = \frac{True\ Positive\ (TP)+True\ Negative\ (TN)}{TP+TN+False\ Positive\ (FP)+False\ Negative\ (FN)} \quad (14)$$

In Eq. (14), TP is the number of COVID-19 samples correctly classified as COVID-19. FP is the number of COVID-19 samples incorrectly classified as healthy. FN is the number of healthy samples incorrectly classified as COVID-19. TN is the number of healthy samples correctly classified as healthy.

In Fig. 4, the accuracy achieved by the different TL-based models implemented on the considered datasets to classify COVID-19 infection risk levels. It observes that the accuracy of the MS-AUNet-MSDATL using CT image dataset is 14% greater than the DDTL, 12.4% greater than the 4SD-TL, and 10.4% greater than the TL-Med models. The accuracy of the MS-AUNet-MSDATL using X-ray image dataset is 16.8% greater than the DDTL, 14.3% greater than the 4SD-TL, and 10.5% greater than the TL-Med models. This is because of localizing COVID-19 diseased tissues and learning more discriminative characteristics from the lung CT scans for infection risk level categorization.

4.2 Precision

It is the amount of categorized COVID-19 examples at TP and FP rates. It is calculated by Eq. (15).

$$Precision = \frac{TP}{TP+FP} \quad (15)$$

Fig. 5 portrays the precision for various TL-based models implemented on the considered databases to classify COVID-19 infection risk levels. It analyses that the precision of the MS-AUNet-MSDATL using CT image dataset is 15.1% higher than the DDTL, 12.8% higher than the 4SD-TL, and 10.5% higher than the TL-Med models for COVID-19 infection risk level categorization. Also, the precision of the MS-AUNet-MSDATL using X-ray image dataset is 17.2% higher than the DDTL, 14.7% higher than the 4SD-TL, and 12.2% higher than the TL-Med models. This ensures that the precision of MS-AUNet-MSDATL is improved compared to the DDTL, 4SD-TL, and TL-Med models on both CT and X-ray images.

4.3 Recall

It is the number of perfectly categorized COVID-19 examples at TP and FN rates. It is determined by Eq. (16).

$$Recall = \frac{TP}{TP+FN} \quad (16)$$

Fig. 6 depicts the recall values of various TL-based models implemented on the considered databases to classify COVID-19 infection risk levels. It addresses that the recall of the MS-AUNet-MSDATL using CT image dataset is 14.8% better than the DDTL, 12.7% better than the 4SD-TL, and 10.5% better than the TL-Med models for COVID-19 infection risk level categorization. Also, the recall of the MS-AUNet-MSDATL using X-ray image dataset is 16.7% better than the DDTL, 12.9% better than the 4SD-TL, and 10.9% better than the TL-Med models. This guarantees that the MS-AUNet-MSDATL can increase the recall for both CT and X-ray images compared to the other existing models for COVID-19 risk level classification efficiently.

4.4 F-measure

It is determined by Eq. (17).

$$F-measure = 2 \times \frac{Precision \cdot Recall}{Precision+Recall} \quad (17)$$

Fig. 7 depicts the recall values of various TL-based models implemented on the considered

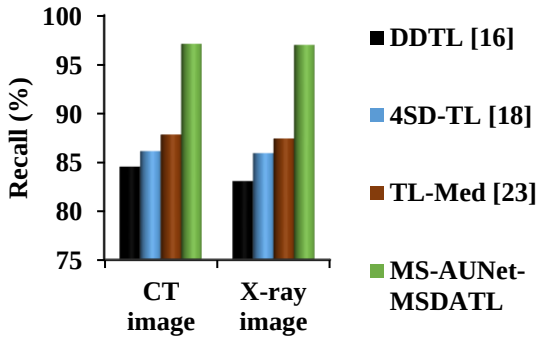

Figure. 6 Comparison of recall

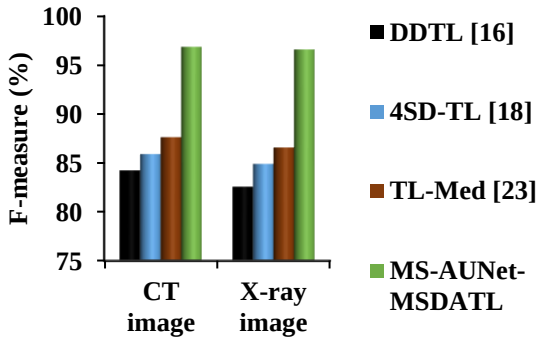

Figure. 7 Comparison of f-measure

databases to classify COVID-19 infection risk levels. It addresses that the recall of the MS-AUNet-MSDATL using CT image dataset is 15% better than the DDTL, 12.7% better than the 4SD-TL, and 10.5% better than the TL-Med models for COVID-19 infection risk level categorization. Also, the f-measure of the MS-AUNet-MSDATL using X-ray image dataset is 17% better than the DDTL, 13.8% better than the 4SD-TL, and 11.6% better than the TL-Med models. This is because of using an ensemble classifier, i.e. CNN-LSTM with TL, whereas the other models employ classical machine learning classifiers for the classification process.

Thus, these findings proved that the proposed MS-AUNet-MSDATL using both CT and X-ray image datasets increases accuracy, precision, recall, and f-measure compared to the DDTL [16], 4SD-TL [18], and TL-Med [23] models efficiently. The proposed MS-AUNet-MSDATL can be useful for physicians to provide an accurate diagnosis by recognizing COVID-19 risk levels.

5. Conclusion

In this study, the MS-AUNet-MSDATL model was developed for COVID-19 disease risk levels categorization. Based on the use of the TL strategy, four different pre-learned CNN structures were employed to hierarchically obtain more relevant and discriminative characteristics from infected ROIs of the lung CT and X-ray scans. The variables of the convolution layers were upheld constantly during the learning procedure. After that, those characteristics were processed by the CNN-LSTM classifier to categorize the risk levels of COVID-19 infection. Also, an ambiguity estimation was performed to predict the classifier's efficiency. Moreover, the success of the presented models was compared with the existing TL models in the literature. The experimental outcomes realized that the MS-AUNet-MSDATL on the chest CT image dataset has 97.34% accuracy, 96.65% precision, 97.07% recall, and 96.86% f-measure compared to the DDTL, 4SD-TL, and TL-Med. Similarly, the MS-AUNet-MSDATL on the chest X-ray image dataset has 97.18% accuracy, 96.21% precision, 96.96% recall, and 96.59% f-measure compared to the DDTL, 4SD-TL, and TL-Med models. In the future, the proposed model will be developed as a big data model to process very large-scale datasets.

Conflict of interest

The authors declare no conflict of interest.

Author contributions

Conceptualization, methodology, software, validation, Jinu Paulson; formal analysis, investigation, Angeline Prasanna; resources, data curation, writing—original draft preparation, Jinu Paulson; writing—review and editing, Jinu Paulson; visualization, supervision, Angeline Prasanna.

References

[1] Z. Yu, A. Razzaq, A. Rehman, A. Shah, K. Jameel, and R. S. Mor, "Disruption in Global Supply Chain and Socio-Economic Shocks: A Lesson from COVID-19 for Sustainable Production and Consumption", *Operations Management Research*, Vol. 15, pp. 233-248, 2022.

[2] N. K. Bagri, R. K. Deepak, S. Meena, S. K. Gupta, S. Prakash, K. Setlur, and S. K. Kabra, "Outcomes of Multisystem Inflammatory Syndrome in Children Temporally Related to COVID-19: A Longitudinal Study", *Rheumatology International*, Vol. 42, No. 3, pp. 477-484, 2022.

[3] B. Jin, R. Singh, S. E. Ha, H. Zogg, P. J. Park, and S. Ro, "Pathophysiological Mechanisms Underlying Gastrointestinal Symptoms in Patients with COVID-19", *World Journal of Gastroenterology*, Vol. 27, No.19, pp. 2341-

2352, 2021.
[4] WHO coronavirus (COVID-19) dashboard. https://covid19.who.int/
[5] M. A. B. Lucien, M. F. Canarie, P. E. Kilgore, G. Jean-Denis, N. Fénélon, M. Pierre, … and P. R. Pardo, "Antibiotics and Antimicrobial Resistance in the COVID-19 Era: Perspective from Resource-Limited Settings", *International Journal of Infectious Diseases*, Vol. 104, pp. 250-254, 2021.
[6] M. A. Kabir, R. Ahmed, S. M. A. Iqbal, R. Chowdhury, R. Paulmurugan, U. Demirci, and W. Asghar, "Diagnosis for COVID-19: Current Status and Future Prospects", *Expert Review of Molecular Diagnostics*, Vol. 21, No. 3, pp. 269-288, 2021.
[7] M. Alhasan and M. Hasaneen, "Digital Imaging, Technologies and Artificial Intelligence Applications during COVID-19 Pandemic", *Computerized Medical Imaging and Graphics*, Vol. 91, pp. 1-22, 2021.
[8] T. A. Soomro, L. Zheng, A. J. Afifi, A. Ali, M. Yin, and J. Gao, "Artificial Intelligence (AI) for Medical Imaging to Combat Coronavirus Disease (COVID-19): A Detailed Review with Direction for Future Research", *Artificial Intelligence Review*, Vol. 55, pp. 1409-1439, 2022.
[9] Z. A. A. Alyasseri, M. A. A. Betar, I. A. Doush, M. A. Awadallah, A. K. Abasi, S. N. Makhadmeh, … and R. A. Zitar, "Review on COVID-19 Diagnosis Models based on Machine Learning and Deep Learning Approaches", *Expert Systems*, Vol. 39, No.3, pp. 1-32, 2022.
[10] E. Benmalek, J. Elmhamdi, and A. Jilbab, "Comparing CT Scan and Chest X-ray Imaging for COVID-19 Diagnosis", *Biomedical Engineering Advances*, Vol. 1, pp. 1-6, 2021.
[11] I. Espallargas, J. J. R. Sevilla, D. A. Rodriguez Chiaradia, A. Salar, G. Casamayor, J. V. Garcia, … and F. Zuccarino, "CT Imaging of Pulmonary Embolism in Patients with COVID-19 Pneumonia: A Retrospective Analysis", *European Radiology*, Vol. 31, No. 4, pp. 1915-1922, 2021.
[12] T. Alafif, A. M. Tehame, S. Bajaba, A. Barnawi, and S. Zia, "Machine and Deep Learning towards COVID-19 Diagnosis and Treatment: Survey, Challenges, and Future Directions", *International Journal of Environmental Research and Public Health*, Vol. 18, No. 3, pp. 1-24, 2021.
[13] V. V. Khanna, K. Chadaga, N. Sampathila, S. Prabhu, R. Chadaga, and S. Umakanth, "Diagnosing COVID-19 Using Artificial Intelligence: A Comprehensive Review", *Network Modeling Analysis in Health Informatics and Bioinformatics*, Vol. 11, No. 1, pp. 1-23, 2022.
[14] T. Zhou, S. Canu, and S. Ruan, "Automatic COVID-19 CT Segmentation Using U-Net Integrated Spatial and Channel Attention Mechanism", *International Journal of Imaging Systems and Technology*, Vol. 31, No. 1, pp. 16-27, 2021.
[15] N. N. Das, N. Kumar, M. Kaur, V. Kumar, and D. Singh, "Automated Deep Transfer Learning-Based Approach for Detection of COVID-19 Infection in Chest X-rays", *IRBM*, Vol. 43, No. 2, pp. 114-119, 2022.
[16] S. Niu, M. Liu, Y. Liu, J. Wang, and H. Song, "Distant Domain Transfer Learning for Medical Imaging", *IEEE Journal of Biomedical and Health Informatics*, Vol. 25, No. 10, pp. 3784-3793, 2021.
[17] D. Singh, V. Kumar, M. Kaur, M. Y. Jabarulla, and H. N. Lee, "Screening of COVID-19 suspected subjects using multi-crossover genetic algorithm based dense convolutional neural network", *IEEE Access*, Vol. 9, pp. 142566-142580, 2021.
[18] A. Abbas, M. M. Abdelsamea, and M. M. Gaber, "4S-DT: Self-Supervised Super Sample Decomposition for Transfer Learning with Application to COVID-19 Detection", *IEEE Transactions on Neural Networks and Learning Systems*, Vol. 32, No. 7, pp. 2798-2808, 2021.
[19] M. Singh, S. Bansal, S. Ahuja, R. K. Dubey, B. K. Panigrahi, and N. Dey, "Transfer Learning–Based Ensemble Support Vector Machine Model for Automated COVID-19 Detection Using Lung Computerized Tomography Scan Data", *Medical & Biological Engineering & Computing*, Vol. 59, No. 4, pp. 825-839, 2021.
[20] S. Ahuja, B. K. Panigrahi, N. Dey, V. Rajinikanth, and T. K. Gandhi, "Deep Transfer Learning-Based Automated Detection of COVID-19 from Lung CT Scan Slices", *Applied Intelligence*, Vol. 51, No. 1, pp. 571-585, 2021.
[21] M. B. Hossain, S. H. S. Iqbal, M. M. Islam, M. N. Akhtar, and I. H. Sarker, "Transfer Learning with Fine-Tuned Deep CNN ResNet50 Model for Classifying COVID-19 from Chest X-ray Images", *Informatics in Medicine Unlocked*, Vol. 30, pp. 1-10, 2022.
[22] N. A. Baghdadi, A. Malki, S. F. Abdelaliem, H. M. Balaha, M. Badawy, and M. Elhosseini, "An Automated Diagnosis and Classification of

COVID-19 from Chest CT Images Using a Transfer Learning-Based Convolutional Neural Network", *Computers in Biology and Medicine*, Vol. 144, pp. 1-17, 2022.

[23] J. Meng, Z. Tan, Y. Yu, P. Wang, and S. Liu, "TL-Med: A Two-Stage Transfer Learning Recognition Model for Medical Images of COVID-19", *Biocybernetics and Biomedical Engineering*, Vol. 42, pp. 842-855, 2022.

[24] M. Gour and S. Jain, "Automated COVID-19 Detection from X-ray and CT Images with Stacked Ensemble Convolutional Neural Network", *Biocybernetics and Biomedical Engineering*, Vol. 42, No. 1, pp. 27-41, 2022.

[25] S. Garg, S. Kumar, and P. K. Muhuri, "A Novel Approach for COVID-19 Infection Forecasting Based on Multi-Source Deep Transfer Learning", *Computers in Biology and Medicine*, Vol. 149, pp. 1-16, 2022.

[26] N. S. Shaik and T. K. Cherukuri, "Transfer Learning Based Novel Ensemble Classifier for COVID-19 Detection from Chest CT-Scans", *Computers in Biology and Medicine*, Vol. 141, pp.1-8, 2022.

[27] K. Simonyan and A. Zisserman, "Very Deep Convolutional Networks for Large-Scale Image Recognition", *arXiv Preprint arXiv:1409.1556*, 2014.

[28] K. He, X. Zhang, S. Ren, and J. Sun, "Deep Residual Learning for Image Recognition", In: *Proc. of the IEEE Conf. on Computer Vision and Pattern Recognition*, pp. 770-778, 2016.

[29] C. Szegedy, W. Liu, Y. Jia, P. Sermanet, S. Reed, D. Anguelov, D. Erhan, V. Vanhoucke and A. Rabinovich, "Going Deeper with Convolutions", In: *Proc. of the IEEE Conf. on Computer Vision and Pattern Recognition*, pp. 1-9, 2015.

[30] D. Singh, V. Kumar, and M. Kaur, "Densely Connected Convolutional Networks-Based COVID-19 Screening Model", *Applied Intelligence*, Vol. 51, No. 5, pp. 3044-3051, 2021.

[31] https://github.com/dara1400/Covid19-Xray-Dataset

[32] Radiopaedia-COVID-19 CT Cases-2020 dataset. www.radiopaedia.org